*Progress In Electromagnetics Research, Vol. 143, 187–206, 2013*

# RADIOMETRIC METHOD FOR EMISSIVITY RETRIEVAL IN HIGH REFLECTIVE MATERIALS

**Marco Canavero*** **and Axel Murk**

IAP, University of Bern, Switzerland

**Abstract**—High reflective materials in the microwave region play a very important role in the realization of antenna reflectors for a broad range of applications, including radiometry. These reflectors have a characteristic emissivity which needs to be characterized accurately in order to perform a correct radiometric calibration of the instrument. Such a characterization can be performed by using open resonators, waveguide cavities or by radiometric measurements. The latter consists of comparative radiometric observations of absorbers, reference mirrors and the sample under test, or using the cold sky radiation as a direct reference source. While the first two mentioned techniques are suitable for the characterization of metal plates and mirrors, the latter has the advantages to be also applicable to soft materials. This paper describes how, through this radiometric techniques, it is possible to characterize the emissivity of the sample relative to a reference mirror and how to characterize the absolute emissivity of the latter by performing measurements at different incident angles. The results presented in this paper are based on our investigations on emissivity of a multilayer insulation material (MLI) for space mission, at the frequencies of 22 and 90 GHz.

## 1. INTRODUCTION

The emissivity of high reflective materials depends on ohmic losses of the surface layer of the reflector; such losses are related to the thickness, roughness and conductivity of this layer and on dielectric losses of protecting surface cover, if present. These losses depend on frequency, incident angle and polarization of the incoming waves.

One way to characterize the losses of a highly reflective sample is to measure the reduction of the $Q$-factor of an open resonator when

*Received 5 August 2013, Accepted 16 October 2013, Scheduled 31 October 2013*

* Corresponding author: Marco Canavero (marco.canavero@iap.unibe.ch).

it is loaded with the material under test. Such a setup can perform relative measurements between a reference mirror and the test sample, at normal or at oblique incident angles [1–3]. The uncertainty of this method is related to the losses of the reference reflector, which can be assessed by reconfiguring the measurement setup in order to characterize reference and resonator losses [1]. The absolute accuracy of the method will then depend on the accuracy to which the setup can be aligned and on the changes of the environmental conditions during the measurements (mainly temperature), requiring a controlled environment for the measuring process. Moreover the measurement results can be affected by undesired standing waves, leading to an overestimation of emissivity of the sample.

Waveguide cavities can also be used to determine emissivity of high reflective low losses samples, by exciting, i.e., in circular cavities, the $TE_{01}$ mode (where one of the cavity walls is the sample under test), and comparing the measured $Q$-factor with the reference one. The advantages of this approach are that the electrical contact between the sample and the other cavity walls has no significant impact on the measured $Q$-factor and that such a setup is very robust and does not require any alignment effort. Drawbacks come from the fact that not-rigid samples are hard to keep taut as cavity walls. In the case of multi-layer insulators and other high reflectivity textiles, the irregularities on the surface that normally happen once the cavity is pressed over the sample surface would lend to erroneous measurements of the $Q$ factor. In the case of our multi-layers insulator, it was still possible to perform a cavity measurement of the superficial layer, keeping it as taut as possible, but this approach results in a rough estimation of the sample emissivity. In resonator or cavity approaches usually one has to also implement external components (such cold loads and switching mirrors) for calibrating the measurements, specifically designed for the given frequency bands, resulting in a complex setup.

Alternative method from the ones described above consists on emissivity estimation from passive radiometric measurements (an example of this approach is reflector tests for the WMAP mission [4]). In such a case a microwave radiometer looks to a cold source through reflections from the high reflective sample under test. Observing the temperature difference between the cold target in direct view or through a reference mirror and the sample it is possible to derive the emissivity of the latter. If this measurement is sensitive to sidelobes contributions from the radiometer optics, and to the stability of the instrument (common phenomena in radiometry), switching between a reference reflector and the sample placed above it will lead to better results in term of accuracy than using the direct view of the cold source

as reference (if the size of the sample and mirror are larger than the instrument beam). Our radiometric method uses cold sky observed through a reflecting mirror as reference cold temperature, which has the advantage that it will not cause any standing waves. Employed radiometers, sample description, test setups and measurement methods are described in the following sections of this work.

## 2. RADIOMETERS DESCRIPTIONS

For our radiometric emissivity retrieval experiment two distinct radiometers have been used: an elevation scanning polarimeter operating in W-band and a dual polarization radiometer operating in K-Band.

The Scanning Polarimetric Imaging Radiometer (SPIRA) is a fully polarimetric imager in the 90–92 GHz band [5]. The instrument can measure simultaneously the 4 Stokes parameters for an observed scene using two orthogonally polarized receiver channels and an analog adding correlation network with 2 GHz of bandwidth. The integration time/pixel is 18 ms while average acquisition time/image and receiver noise temperature are respectively 5 min and 600 K. The antenna consists of a dual polarized corrugated feed horn and a 90°-axis parabolic reflector with an effective focal length of 70 cm and a projected aperture of 45 cm, with a full-with-half-maximum beam width of about 0.5°. Sidelobes for both $H$ and $E$ planes are below −20 dB. Fig. 1 gives a schematic overview of the SPIRA polarimeter.

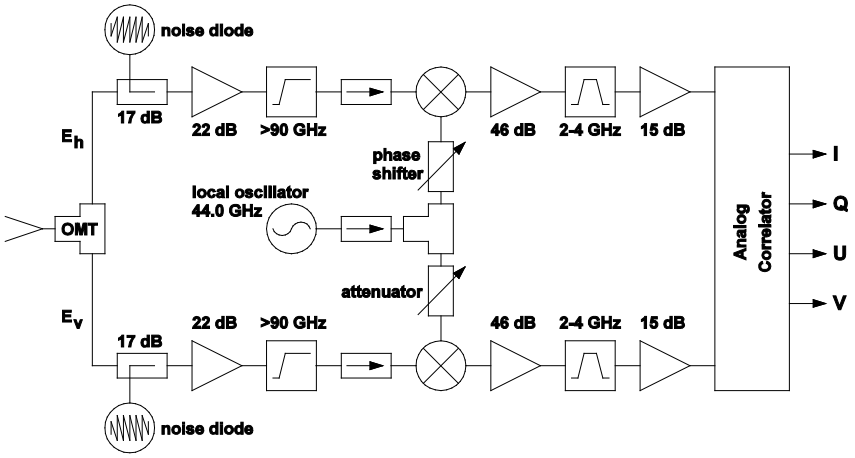


**Figure 1.** Block diagram of SPIRA receiver.

It consists of two heterodyne receiver chains, which are both connected to the feed horn through an orthomode transducer (OMT). In each channel an additional noise signal from a switchable noise diode can be injected through a directional coupler, and is used together with an ambient temperature blackbody calibration target to calibrate the gain and system temperature of the receiver at the beginning of each elevation scan. Each receiver's RF channel consists of low noise RF amplifier following the coupler for the noise diode calibration, an high pass filter, subharmonic Schottky mixers (SSB). The latter are fed by a common local oscillator (44 GHz) to ensure the phase coherence between the two receiver channels. Variable attenuators and a phase shifter in the local oscillator path ensure an optimal pumping of the mixers and fine adjustment of the phase shift.

The down-converted signals are amplified by low-noise IF amplifiers and band limited to frequencies between 2 and 4 GHz before entering the analog correlator network (formed by 90° and 180° hybrid couplers and phase shifters). The output channels of the analog correlator network provide the four Stokes parameters ($I$, $Q$, $U$ and $V$) and the horizontal and vertical brightness temperatures [5].

The other radiometer involved in our test setup is the Middle Atmospheric Water Vapor Radiometer MIAWARA-C [6, 7]. It is a ground-based microwave radiometer designed for middle atmospheric water vapor retrievals, especially for use on measurement campaigns for both atmospheric case studies and instrument intercomparisons. More specifically, MIAWARA-C has been designed to measure the rotational emission line of water vapor at 22.235 GHz. Its optical system consists of a very compact choked Gaussian horn antenna and a parabolic off-axis mirror with a resulting HPBW of 5° and side lobes below −40 dB [6]. The receiver of MIAWARA-C (See Fig. 2) consists of two identical receiver chains for dual polarization observations. In such a setup the incident radiation is split into vertical and horizontal polarization by an orthomode transducer (OMT) placed immediately after the antenna. The two polarized signals are processed in the two identical receiver chains and then analyzed in the digital Fast Fourier Transform (FFT) spectrometer with a spectral resolution of 30.5 kHz and a usable bandwidth of 400 MHz in each polarization [7].

For the absolute calibration two black body targets are measured: a microwave absorber at ambient temperature used as the hot load and the sky at an elevation angle of 60°. The instrument shows good performances in term of internal noise. The noise temperatures for both channels (vertical and horizontal polarizations) are respectively 133 and 137 K.

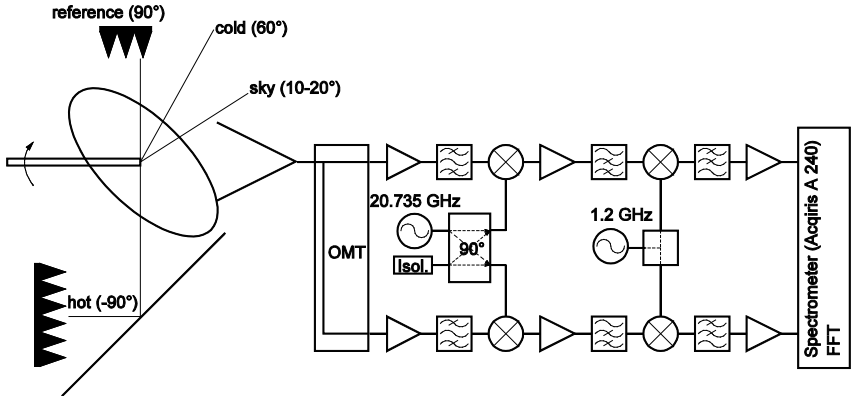


**Figure 2.** Block diagram of MIAWARA-C radiometer.

## 3. SAMPLE DESCRIPTION

The main test sample for our emissivity retrievals is a 0.8 m × 0.8 m sheet of multilayer insulation (MLI), provided by TAS France and manufactured by IberEspacio. The front side of this MLI assembly consists of a Black Kapton foil with dark gray color. It has 1 mm diameter perforations on a regular 10 mm pitch and a thickness of 25 μm (Fig. 3). The backside of the MLI assembly has a shiny metallic finish.

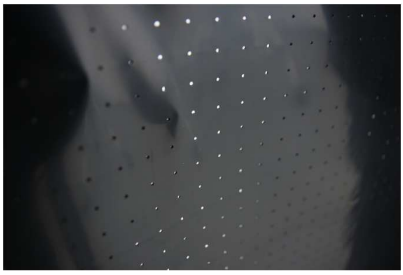

**Figure 3.** Detail of MLI sample (front side).

DC measurements showed a high conductivity on the metalized side and specific contact resistance of approximately 4 kΩ/cm$^2$ between the black side (front) and the metallization (back).

The MLI will be used as a thermal blanket on the GMES Sentinel-3 satellite next to a passive microwave radiometer (MWR) operating at 23.8 and 36.5 GHz for atmospheric sounding. Part of the spillover

at the MWR main reflector will be reflected at the MLI. In order to correct a potential bias of the MWR observations it is important to know the emissivity of the MLI.

If the MLI has a sufficiently low emissivity it can be considered, in the radiometric spillover correction, as a perfect reflector. Otherwise its thermal emission needs to be included in the system model, leading to a larger calibration uncertainty because of the unknown MLI temperature.

## 4. EMISSIVITY RETRIEVAL AND TEST SETUP

As previously mentioned, for our experiment we used different radiometers at different frequencies, in order to measure the brightness temperature ($T_B$) or a power measurement of the incoming wave reflected by the sample when pointed at a cold target, which is the zenith cold sky radiation in our case. Then the effective brightness temperature $T_B$ will depend on the cold sky temperature $T_c$, the ambient temperature $T_{amb}$ of the sample and its emissivity $\varepsilon$:

$$T_B = T_{amb}\varepsilon + T_c(1-\varepsilon) \tag{1}$$

This equation relates the emissivity of materials to the measured brightness temperature. For a plane-parallel atmosphere and the assumption that the atmosphere is isothermal, $T_c$ depends on the angle of the incoming wave $\vartheta_c$ (zenith angle in our case) and the zenith opacity $\tau_0$, and is calculated, using the radiative transfer theory in the Rayleigh-Jeans approximation for plane-parallel and isothermal atmosphere, through the following formula:

$$T_c = T_{atm}\left(1 - \exp\left(\frac{-\tau_0}{\cos\vartheta_c}\right)\right) + T_0 \exp\left(\frac{-\tau_0}{\cos\vartheta_c}\right) \tag{2}$$

where $T_0$ is the cosmic background radiation and $T_{atm}$ the mean atmospheric temperature. Zenith opacity $\tau_0$ can be obtain on-field by an elevation scanning radiometer performing a tipping curve measurement and depends on atmospheric conditions [8].

If it is not possible to determine $T_c$, a relative method can be applied in order to retrieve the emissivity of the sample, alternating the latter with a reference mirror during the measurement phase [9]. In this case an absolute calibration or the knowledge of the actual sky temperature is not required.

In our case, we used MIAWARA-C pointed towards zenith using an extended aluminum reflector at an incidence angle of 45°. Then a cycle of 5 observations with the radiometer reflector switching between the reference aluminum mirror and the zenith direction has

been perform. Before and after the cycle, an ambient temperature load has been measured. Then a new measurement cycle has been performed exchanging the reference mirror with the MLI sample, and the entire procedure (reference and MLI) was repeated several times to check the measurement repeatability (Fig. 4). Assuming that the reflectivity of the reference reflector is 100% and that the sample and the internal load have the same physical temperature, the emissivity can be calculated using:

$$\varepsilon = \frac{V_{sam} - V_{ref}}{V_{abs} - V_{ref}} \tag{3}$$

where $V_{sam}$ is the value (voltage or temperature) retrieved from the sample under test, and $V_{ref}$ and $V_{abs}$ are repectively the reference (aluminum mirror) and the internal load ones. The dominant uncertainty source in this approach is the unknown reflectivity of the reference reflector, which will be discussed in more detail in the next section. Since the geometry remains the same with and without the MLI sample, Sidelobes and spillover effects should not affect the estimated emissivity. In this sense, the very low level of sidelobes in MIAWARA-C will prevent relevant error contribution. By comparing the sample measurements with a direct observation of the sky at the zenith angle, instead, could lead to an error in the emissivity estimation


**Figure 4.** Picture of the test setup for the emissivity measurements using MIAWARA-C radiometer. The MLI sample covers the Aluminum reference reflector about 50% of the measurement time. A weather station is installed nearby the instrument (left).

if radiometer sidelobes level is not negligible. The diameter of the radiation pattern of the radiometers, relative to the distance from the targets, has to be considered in order to avoid a partial beam filling from the surrounding environment (this is particularly import if the sample and the reference mirror have different dimensions). Other possible sources of error which could lead to a wrong estimation of emissivity is atmospheric condition change and the sun position relative to the sample. The latter can rapidly change the temperature of the sample in case of direct exposition. The sensitivity of the measurement is also limited by the noise and instabilities of the radiometer.

In the case of a scanning polarimeter like SPIRA, from (1) we can also derive the emissivity (for each polarization) as:

$$\varepsilon_b = \frac{T_b - T_{sky}}{T_{amb} - T_{sky}} \tag{4}$$

As mentioned before, $T_{sky}$ can be retrieved by a tipping curve, and $T_{amb}$ is the ambient temperature while $T_b$ is the brightness temperature for the considered polarization. In order to accurately intercept the zenith cold radiation, reflected by the plates, the samples must be aligned at a certain angle $\beta$ relatively to the basement. A scheme of the setup is shown in Fig. 5.

Where:

$\beta$: angle between incident radiation from zenith and the normal

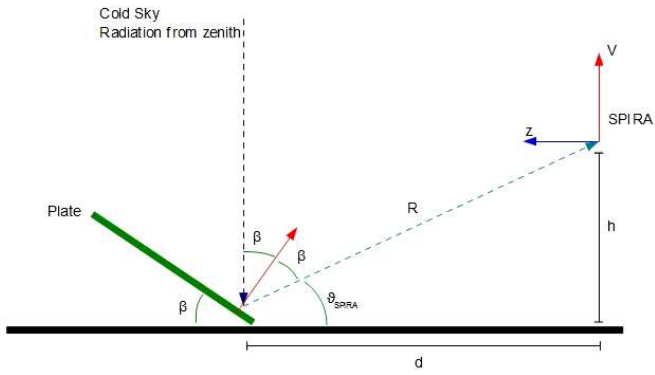


**Figure 5.** Scheme of the test setup for the emissivity measurements using a scanning radiometer like SPIRA. Height and distance of the instrument from the sample is taken into account to determine the correct tilting angle of the sample in order to intercept the cold sky radiation at zenith.

axis of the plate.

$\vartheta_{\mathrm{SPIRA}}$: elevation angle of the radiometer where the zenith ray is reflected (0° for the horizon).

$R$: path length of the reflected radiation.

$h$: height of SPIRA receiver from basement.

$d$: distance between SPIRA and the plate (bottom).

Observing Fig. 5, $\beta$ is also the desired inclination angle of the plate and can be expressed as:

$$\beta = \frac{90^\circ - \vartheta_{\mathrm{SPIRA}}}{2} \tag{5}$$

Using simple trigonometric laws:

$$h = R \sin \vartheta_{\mathrm{SPIRA}} \tag{6}$$

$$d = R \cos \vartheta_{\mathrm{SPIRA}} \tag{7}$$

$$R = \sqrt{h^2 + d^2} \tag{8}$$

We obtain:

$$\sin \vartheta_{\mathrm{SPIRA}} = \frac{h}{R} = \frac{h}{\sqrt{h^2 + d^2}} \tag{9}$$

$$\cos \vartheta_{\mathrm{SPIRA}} = \frac{d}{\sqrt{h^2 + d^2}} \tag{10}$$

From which we can calculate $\beta$ angle.

## 5. CHARACTERIZATION OF THE REFERENCE MIRROR

In order to obtain the absolute emissivity of the sample from the relative measurement, the reference plate emissivity has to be calculated. The power reflection coefficient for TE and TM planes in case of a reflected wave on a metal surface are given by [1]:

$$r_{\mathrm{TE}} = 1 - \frac{4R_s \cos(\vartheta)}{Z_0} \tag{11}$$

$$r_{\mathrm{TM}} = 1 - \frac{4R_s}{\cos(\vartheta) Z_0} \tag{12}$$

where $Z_0 = \mu_0/\varepsilon_0$ is the vacuum impedance, $\vartheta$ is the incidence angle and $R_s$, the surface resistance of the metal, is given by:

$$R_s = \sqrt{\frac{\pi \nu \mu_0}{\sigma}} \tag{13}$$

Here, $\nu$ is the frequency, $\sigma$ is the DC conductivity of the material and $\mu_0$ is the vacuum permeability. For a metal plate, from the model in (11), (12), the emissivity can be calculated as:

$$\text{TE case:} \quad \varepsilon_{\text{TE}} = \frac{4R_s \cos(\vartheta)}{Z_0} \tag{14}$$

$$\text{TM case:} \quad \varepsilon_{\text{TM}} = \frac{4R_s}{Z_0 \cos(\vartheta)} \tag{15}$$

Since $R_s$ is independent of the incident angle, it is possible to derive it by performing an emissivity retrieval (2) at two different angles $\theta_{1,2}$ of incidence between the radiometer and the reference plate, pointing at the same reference (in our case, the Zenith direction), in the following way:

$$\text{TE case:} \quad R_s = \frac{Z_0(\varepsilon_1 - \varepsilon_2)}{4(\cos(\vartheta_1) - \cos(\vartheta_2))} \tag{16}$$

$$\text{TM case:} \quad R_s = \frac{Z_0(\varepsilon_1 - \varepsilon_2)}{4(\sec(\vartheta_1) - \sec(\vartheta_2))} \tag{17}$$

The estimated thermal sensitivity of the radiometer required for the characterization of the reference metal plate can be calculated as follow (TE case). From (4) we have:

$$\varepsilon_1 - \varepsilon_2 = \frac{T_{b1} - T_{sky}}{T_{amb} - T_{sky}} - \frac{T_{b2} - T_{sky}}{T_{amb} - T_{sky}} = \frac{T_{b1} - T_{b2}}{T_{amb} - T_{sky}} \tag{18}$$

where the indexes denote two retrievals at two different incident angles, assuming that $T_{sky}$ and $T_{amb}$ do not vary during the measurements. The emissivity difference, according to (17), is also:

$$\varepsilon_1 - \varepsilon_2 = \frac{\Delta T}{T_{amb} - T_{sky}} = \frac{4R_s(\cos(\vartheta_1) - \cos(\vartheta_2))}{Z_0} \tag{19}$$

Then we have:

$$\Delta T = \frac{4R_s(T_{amb} - T_{sky})(\cos(\vartheta_1) - \cos(\vartheta_2))}{Z_0} \tag{20}$$

Which can be used to estimate the necessary sensitivity of the instrument in order to measure the emissivity difference. The required integration time can be then estimated considering the radiometer equation:

$$\Delta T \approx \left( \frac{T_{sam} + T_N}{\sqrt{B\tau}} \right) \tag{21}$$

where $T_{sam}$ is the temperature of the target, $T_N$ is the noise temperature of the radiometer, $B$ is the receiver bandwidth. Broad

receiver bandwidth, accurate choice of the two incident angles $\vartheta_1$ and $\vartheta_2$, and gain stability can reduce the required $\tau$.

It is important to emphasize here that also gain fluctuations and drifts, which affects the quality of the measurement for the characterization of the reference mirror, are proportional to the length of the observation, then a trade-off between long integration time and low drifts has to be done. Moreover, a long $\tau$ could make not valid anymore the assertion in (18). It is then very important to perform the measurements during stable weather conditions within a short time window.

The sun position along the measurements time is also relevant because the temperature of the sample and the reference mirror can rapidly increase due to direct sun exposition. We recommend to choose a proper orientation of the test setup in order to avoid the passage of the sun in front of the target.

The minimum integration time in order to measure the emissivity variation at the two different incident angles can then obtained as:

$$\tau > \frac{1}{B}\left(\frac{T_{sam} + T_N}{\Delta T}\right)^2 \tag{22}$$

With estimated $\Delta T$ from (20).

A plot of the required thermal sensitivity of the radiometer, for emissivity retrievals method, at different frequencies and DC conductivity is shown in Fig. 6.

For a radiometer like MIAWARA-C, with a receiver bandwidth of 400 MHz, a central frequency of 22.2 GHz and noise temperature $T_N$ of 133 K, we need a minimum integration time of 0.2 seconds in order to characterize the reference mirror at the two incident angles $\vartheta_1 = 30°$ and $\vartheta_2 = 45°$.

## 6. MEASUREMENTS RESULTS

In the following, we present some of the results achieved during our measuring campaign.

The emissivity measurements were conducted outdoor, on the roof of our institute, in clear sky weather condition. This is a very important prerequisite, as we already stated, clouds passing at the zenith will seriously compromise the effectiveness of the retrievals.

For the measurements performed with SPIRA radiometer, we used the setup described in Fig. 5. Using the formulas from (4) to (8) and having $h = 1.68$ m and $d = 13.9$ m, we obtain that the zenith angle is intercepted by our setup for $\vartheta_{\mathrm{SPIRA}} = -6.9°$, when the sample is inclined at an angle $\beta = 41.5°$. The central frequency was 91 GHz with

an integration time per elevation point set at 18 ms. Before starting the emissivity measurements, a tipping curve scan has been performed for calibration purpose (Fig. 7).

The combination of data coming from tipping curve and the local weather station is then used to obtain the noise diode temperature $T_{ND}$ for each of 6 channels of SPIRA, zenith opacity $\tau_0$ and atmosphere temperature $T_{atm}$. The brightness temperature at 90° is taken as our cold sky radiation reference $T_{sky}$. For the day of measurements we obtained:

$$\tau_0 = 0.03; \quad T_{atm} = 254.38\,\mathrm{K}; \quad T_{sky}(\text{zenith}) = 10.76\,\mathrm{K}$$

The tipping curve has a considerably flat brightness temperature in the elevation range of 85° to 95°. Then the error in tilting the reference mirror and the sample ($\beta$ angle) is negligible if it is in the order of ±1°. In our case the accuracy was far beyond this level and equal to ±0.2°.

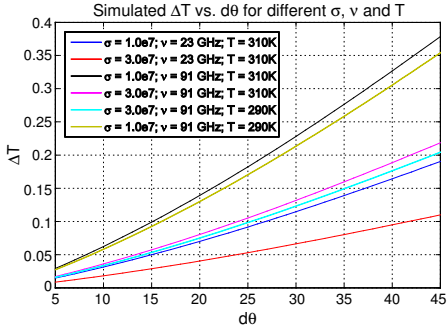


**Figure 6.** Temperature sensitivity plot for different frequencies, DC conductivities and temperatures (TE case). In this plot $\vartheta_1 = 30°$, $\vartheta_2 = \vartheta_1 + d\vartheta$.

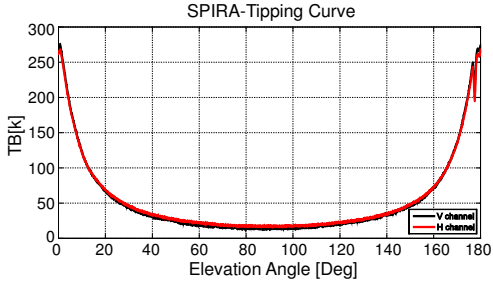


**Figure 7.** SPIRA tipping curve for the measurement day.

The cold sky radiation is expected to be unpolarized but, due to non linearity in the receiver, a small offset in the tipping curves ($V$ and $H$ channels) is visible. This could lead to errors in the emissivity estimation for the two polarizations. Due to the unpolarized nature of the cold sky radiation, we assume the average of the two as our tipping curve from which we calculate $T_{sky}$.

The next step is to perform one dimensional scans (see Fig. 8) of the reference mirror and the sample under test (in our case the MLI foil). In order to have a reference of the cold sky radiation, each one-dimensional SPIRA scan covers an elevation range from 95° to −45° (Zenith direction is at 90°).

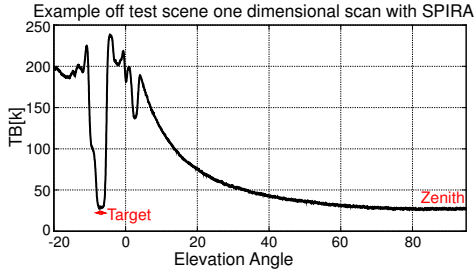


**Figure 8.** SPIRA 1-Dimensional scan of the test scene ($V$ channel). In the specific case, horizontal brightness temperature with Aluminum reference mirror as target.

Figure 9 shows measured intensities of the aluminum plate and Black Kapton MLI (both sides). As reference the zenith temperature value from tipping curve ($T_{sky} = 10.76\,\mathrm{K}$ at zenith angle, Fig. 6) is assumed.

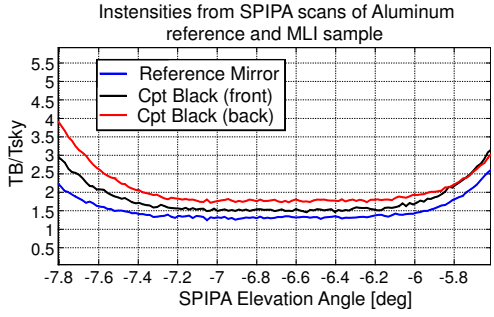


**Figure 9.** Intensities retrieved by SPIRA for the aluminum reference mirror and the MLI front and metallized back ($V$ channel).

**Table 1.** Measured emissivity for MLI and Aluminum plate at 91 GHz.

| **Sample** | $\varepsilon_{\mathbf{h}}$ | $\varepsilon_{\mathbf{v}}$ |
|---|---|---|
| Aluminum plate | $0.014 \pm 1.2\%$ | $0.024 \pm 1.9\%$ |
| MLI Front | $0.02 \pm 1.6\%$ | $0.036 \pm 3.2\%$ |
| MLI Back | $0.028 \pm 2.2\%$ | $0.053 \pm 4.6\%$ |

The retrieved intensities for Aluminum plate and MLI have their minimum values in the instrument elevation range between $-7°$ and $-6.5°$, which is consistent with the calculated angle $\vartheta_{\mathrm{SPIRA}}(= -6.9°)$.

Using (4) the emissivities of the sample and the reference mirror has been estimated. In our calculation we assumed $T_{sky} = 10.76\,\mathrm{K}$, $T_{sam}$ as ambient temperature at measurement time (287.25 K), obtaining the results reported in Table 1.

The results show that the Black Kapton MLI has a relative low emissivity, while the reference mirror has a higher emissivity than expected. Uncertainties of the results comes from: the SPIRA sidelobes contribution to the measurement, from the surrounding environment, during an elevation scan which vary from $-6°$ to $90°$ in elevation; gain fluctuation of the instrument, cross polarization effects in the receiver OMT and the spillover at the target (reference mirror or sample). Moreover, at the end of our measuring cycle, the sun was approaching the direct view of the mirror, which could also lead to an overestimation of the emissivity. While some of these contributions are difficult to characterize, the error margins in Table 1 could represent an underestimation of the real errors.

Using the physical optics software GRASP®, we simulated the effect of the spillover at the SPIRA central frequency (91 GHz) on the target. Concerning the system optic, an ideal Gaussian beam feed horn with edge taper and taper angle from SPIRA datasheet [5], combined with a parabolic off-axis reflector, has been used. A rectangular reflector, of size $0.8 \times 0.8\,\mathrm{m}$ (same size of the MLI) at distance $R$ from the instrument (14 m), represented our simulated target.

The results of our simulations show a spillover $s_p$ at the parabolic reflector of $\approx 2.1\%$ and at the target of an extra 1%. Fig. 10 shows the simulated power distribution on the target reflector while Fig. 11 shows a z-cut of the incident field.

While the spillover at the antenna is the same in both zenith and sample observations and is then negligible, the second one, which occurs only at the sample may considerably effects the value of the retrieved emissivity.

Considering (1), the brightness temperature $T_B$ is here the

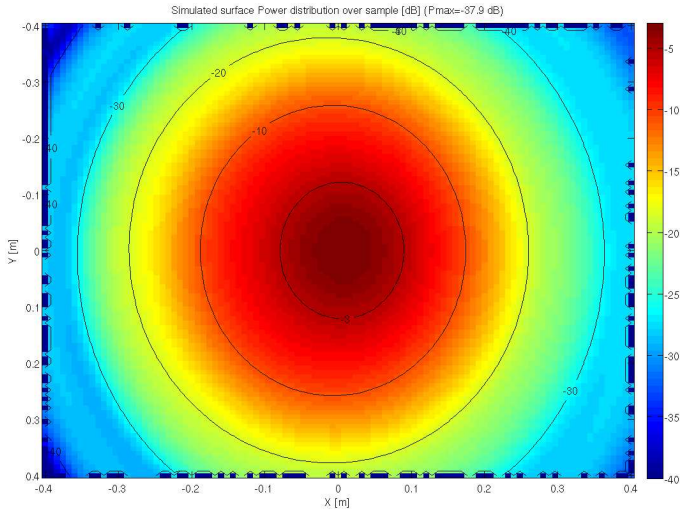


**Figure 10.** Simulated Power distribution on target surface. The size of the plate is the same as the MLI ($0.8 \times 0.8\,\mathrm{m}$). The asymmetry between $X$ and $Y$ directions is given by the tilted angle of the sample, pointing at zenith direction.

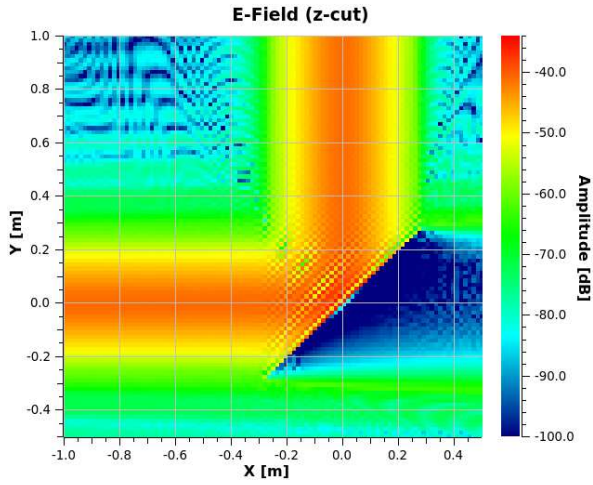


**Figure 11.** $E$-Field cut along the propagation axis ($z$ direction). The target is centered around coordinates $(0, 0)$ and is tilted at 45°. The spillover at the edge of the mirror is noticeable.

**Table 2.** Emissivity for MLI and Aluminum plate at 91 GHz after the spillover correction.

| **Sample** | $\varepsilon_{\mathbf{h}}$ | $\varepsilon_{\mathbf{v}}$ |
|---|---|---|
| Aluminum plate | 0.004 | 0.014 |
| MLI Front | 0.01 | 0.026 |
| MLI Back | 0.018 | 0.044 |

effective temperature at the sample (or at the reference mirror). The measured temperature $T_{B,meas}$ is a combination of the latter and the surrounding environment, due to the spillover effect and can be expressed in the following way:

$$T_{B,meas} = (1 - s_p)T_{B,eff} + s_p \left[T_{amb}\varepsilon_{env} + T_c(1 - \varepsilon_{env})\right] \tag{23}$$

Assuming that the environment can be approximated as an absorber ($\varepsilon_{env} \to 1$) the effective brightness temperature of sample, taking into account the spillover effect, can be calculated as:

$$T_{B,eff} = \frac{T_{B,meas} + s_p T_{amb}}{1 - s_p} \tag{24}$$

Once the correction to the brightness temperatures, due to spillover, is applied, the emissivities are retrieved using (4) (Table 2).

Due to the ideal feed horn used in our simulation, the result has to be considered as an underestimation of the spillover at the target, and the emissivity in Table 2 are consequently overestimated. Furthermore, as a result of the nature of Gaussian beams propagation, a closer distance between the SPIRA antenna and the sample could have improved the spillover efficiency of the measurement setup. A similar improvement is reached by increasing the size of the target. Generally, due to irregularities of any real optical system, an analytic approach through simulation tools is strictly advised in order to optimize the emissivity retrieval setup and to characterize the spillover.

The emissivity retrieval has also been performed using MIAWARA-C radiometer at 22.3 GHz using a very simple setup as shown in Fig. 4. Aluminum reference plate and MLI sample, pointing at the zenith, have been alternated every measurement cycle. Each cycle consisted of a hot load measurement, followed by 5 sequences of an alternating observation through zenith direction and towards the target, concluded by another hot load measurement. The integration time for each measurement was approximately 14 seconds and the distance between the instrument and the sample was approximately 2 m. An example of measurement cycle is shown in Fig. 12.

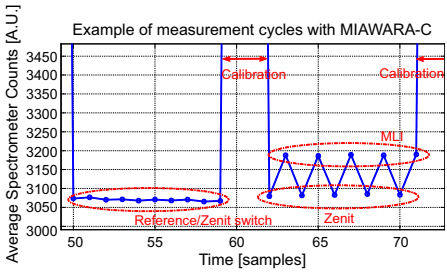


**Figure 12.** Example of measurement cycles using MIAWARA-C. Mean values from the 12 k channels of the instrument. Each sample is a result of an integration time of 14 seconds ($V$ channel).

Several measurement cycles have been accomplished for incident angles (from the plate and MLI normal) of 45° and 60°, resulting in an elevation angle for the instrument of 0° and 30°. The latter has to be taken into account during data processing in order to compensate the polarization mixing due to the radiometer reflector rotation. The flat nature of the sky radiation around the zenith angle allowed us to point the samples at the cold sky with negligible alignment error. The direct observation of the zenith has been useful to compensate any gain fluctuation in the receiver (assuming that the sky temperature does not change in a measurement cycle) and the measured spectrum in MIAWARA-C appears to be consistent between different measurements cycles, showing good performances in term of stability and repeatability. Due to the nature of the measurement cycle, a sequence made of zenith and either sample or reference mirror observations are performed. Calling the sample spectrum, at measuring time $i$, $S_{sam,i}$ and the zenith spectrum $S_{zen}$, we calculate the best possible averaging $S_{sam}$ among an entire cycle composed by $N$ position switches, by performing a first order compensation of gain drifts, in the following way:

$$S_{sam} = \frac{1}{N}\sum_{1}^{N}\left(S_{sam,i} - \frac{S_{zen,i-1} + S_{zen,i+1}}{2}\right) \tag{25}$$

Using (3) we then calculate the relative emissivities at each spectrum line, averaging the results, for both TE and TM polarizations. This process is repeated for different cycles, in order to check the repeatability of the measurements and at different angles. The results are reported in Table 3.

Repeatability of the measurement along different cycles is acceptable and the results look consistent. The estimated emissivity of

**Table 3.** Measured emissivity for MLI at 22.3 GHz (relative to Aluminum reflector).

| **Sample (retrieval)** | **Incident angle** | $\varepsilon_{\mathbf{TM}}(\pm\mathbf{0.3}\%)$ | $\varepsilon_{\mathbf{TE}}(\pm\mathbf{0.3}\%)$ |
|---|---|---|---|
| MLI front (1) | 45° | 0.0196 | 0.0098 |
| MLI front (2) | 45° | 0.0195 | 0.0097 |
| MLI front (3) | 45° | 0.0195 | 0.0095 |
| MLI back (1) | 45° | 0.0162 | 0.0084 |
| MLI front (1) | 60° | 0.0231 | 0.0138 |
| MLI front (2) | 60° | 0.0230 | 0.0139 |
| MLI front (3) | 60° | 0.0249 | 0.0144 |
| MLI back (1) | 60° | 0.0188 | 0.0106 |

**Table 4.** Measured emissivity for Aluminum plate at 22.3 GHz.

| **Incident angle** | $\varepsilon_{\mathbf{TM}}$ | $\varepsilon_{\mathbf{TE}}$ |
|---|---|---|
| 45° | 0.0009 | 0.688e-3 |
| 60° | 0.0013 | 0.554e-3 |

the reference mirror, calculated with (3) using the zenith measurement as reference, are shown in Table 4.

For the characterization of the reference plate, we used (16), obtaining a surface resistivity $R_s$:

$$R_s = \frac{Z_0(\varepsilon_1 - \varepsilon_2)}{4(\cos(\vartheta_1) - \cos(\vartheta_2))} = \frac{377(\varepsilon_1 - \varepsilon_2)}{4(\cos(45°) - \cos(60°))} = 0.061\ \Omega \cdot \mathrm{m}$$

The same result is achieved using the TM Equation (17).

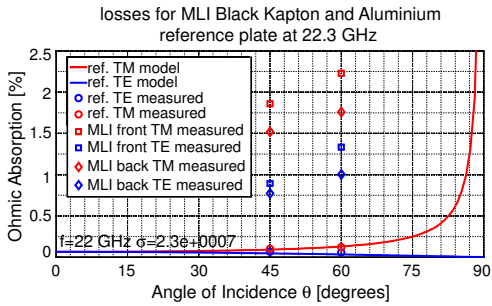


**Figure 13.** Simulated reference mirror losses (lines) and the emissivity results (points) for the reference mirror and the MLI at incident angles of 45° and 60°.

From the definition of $R_s$ (13), at the given frequency $\nu = 22.2\,\text{GHz}$, the DC conductivity $\sigma$ of our reference plate is:

$$\sigma_{REF} = 2.35 \cdot 10^7 \tag{26}$$

This is consistent with aluminum conductivity range found in datasheets. Fig. 13 resumes the results of the emissivity measurement with MIAWARA-C. The retrieved reference mirror emissivity is consistent with the model in (11), (12). MLI absolute losses are in the range of 0.7%–2.5%.

## 7. SUMMARY

The proposed method for the characterization of the reference mirror and the emissivity retrieval of high reflectivity samples proved to be feasible. Using an adequate integration time combined with a radiometer having a low noise temperature, we have been able to measure the absolute emissivity for high reflective materials. The DC conductivity retrieved at 22 GHz is within the expected values for an aluminum (or aluminum alloy) plate. MIAWARA-C radiometer proved to be suitable for the reference characterization, thanks to its low noise temperature and extremely low sidelobes. It is not possible to derive any further conclusions on the MLI Black Kapton, but the good results achieved with the reference mirror at 22 GHz and measurement repeatability allow us to assume that the real emissivity of the MLI is close to our results. The repeatability of the measurements (Table 3) shows that fluctuations in atmosphere conditions and temperature do not constitute a problem for our emissivity retrievals, due to the short measurement cycle time (in the order of 2 minutes) and the relative method used to calculate the losses.

Considering the measurements at 91 GHz, the retrieved emissivity of the aluminum is higher than expected by models. We assume that the results in this frequency range have been overestimated due to a combination of factors: the distance between the instrument and the sample which could lead to a poor beam filling factor; the difficulty of properly pointing the instrument at the center of the target; the higher side lobes and spillover effects of SPIRA compared to MIAWARA-C; the noise temperature of the instrument and the relative short integration time for each point of an elevation scan; the cross polarization effect in the receiver. Moreover, the measurement cycle with SPIRA have been done along an entire day, and weather and temperature conditions of the sample could have changed consistently along time.

## ACKNOWLEDGMENT

The development work for SPIRA radiometer has been funded by Armasuisse W+T under Project No. R-3210/040-11.

## REFERENCES

1. Kasparek et al., "Measurements of ohmic losses of metallic reflector at 140 GHz using a 3-mirror technique," *International Journal of Infrared and Millimeter Waves*, Vol. 22, No. 11, 1695–1707, 2001.
2. Yang, B. B., et al., "A high-Q terahertz resonator for the measurement of electric properties of conductors and low-loss dielectrics," *IEEE Transactions on Terahertz Science and Technology*, Vol. 2. No. 4, 449–459, 2012.
3. Van Klooster, K., et al., "Results of reflection loss measurement of sample material for radio astronomy telescope antenna for planck project," *14th Internation Crimean Conference on Microwave and Telecom Technologies*, 753–755, 2004.
4. Butler, N. R., "Emissivity measurements of MAP satellite optics," Physics Dpt. Senior Thesis, Princeton University, 1998.
5. Duric, A., A. Magun, A. Murk, C. Mätzler, and N. Kämpfer, "The fully polarimetric imaging radiometer SPIRA at 91 GHz," *IEEE Transactions on Geoscience and Remote Sensing*, Vol. 46, No. 8, 2323–2336, 2008.
6. Straub, C., A. Murk, and N. Kämpfer, "MIAWARA-C. A new ground based water vapor radiometer for measurement campaigns," *Atmospheric Measurement Techniques*, Vol. 3, 1–15, 2010.
7. Tschanz, B., et al., "Validation of middle atmospheric campaign-based water vapor measured by the ground-based microwave radiometer MIAWARA-C," *Atmospheric Measurement Techniques Discussions*, Vol. 6, 1311–1359, 2013.
8. Stähli, O., et al., "A surface-based method for water vapour and liquid clouds using a scanning radiometer at 91 GHz," *IEEE transaction on Geoscience and Remote Sensing*, Vol. 40, No. 9, 3273–3280, 2011.
9. Skou, N., "Measurement of small antenna reflector losses for radiometer calibration target," *IEEE Transactions on Geoscience and Remote Sensing*, Vol. 35, No. 4, 967–971, 1997.